Chapter 8
Surface Strain on Bone and Sutures in a Monkey Facial Skeleton: An In Vitro Approach and its Relevance to Finite Element Analysis

Qian Wang, Paul C. Dechow, Barth W. Wright, Callum F. Ross, David S. Strait, Brian G. Richmond, Mark A. Spencer, and Craig D. Byron

Contents

8.1 Introduction and Background

There have been a number of studies on strain across craniofacial sutures in the past two decades, especially the work on pigs in Herring's lab (Herring and Mucci, 1991; Herring, 1993; Rafferty and Herring, 1999; Herring and Rafferty, 2000; Herring and Teng, 2000; Rafferty et al., 2003), which have identified important mechanical

Q. Wang
Division of Basic Medical Sciences, Mercer University School of Medicine, 1550 College St., Macon, GA 31207
e-mail: WANG_Q2@Mercer.edu.

C. Vinyard et al. (eds.), *Primate Craniofacial Function and Biology*,
DOI: 10.1007/978-0-387-76585-3_8,

features of patent sutures. However, little research has been done on the structure, biomechanics, or ontogenetic changes of facial sutures in primates. Species-specific bone cell dynamics might produce different patterns of suture and bone biomechanics in different species (Carmody et al., 2006), so an investigation of primates is warranted. This study investigates the strain distribution across sutures in a primate skull.

In vivo experiments have demonstrated that sutures are strain dampeners, where strain magnitudes are significantly greater across sutures than on the surrounding bony surfaces. Many studies have amply born this out since strains over sutures were first measured by Behrents and colleagues (Behrents et al., 1978; Oudhof and van Doorenmaalen, 1983; Smith and Hylander, 1985; Herring and Mucci, 1991; Herring, 1993; Jaslow, 1990; Jaslow and Biewener, 1995; Rafferty and Herring, 1999; Herring and Rafferty, 2000; Herring and Teng, 2000; Liu and Herring, 2000; Rafferty et al., 2003; Lieberman et al., 2004).

Furthermore, there are many variations in sutural morphology (e.g., short, long, straight, "zigzag", direct edge-to-edge contact, overlapping) (Herring, 1972), configuration patterns (e.g., at the nasal and pterion areas) (Wang et al., 2006a, b), and the biomechanical properties of sutures can differ even within a single individual. For example, three facial sutures in rabbits, the pre-maxillo-maxillary suture, the naso-frontal suture, and the zygomatico-temporal suture and adjacent sutural mineralization fronts in rabbits have different elastic properties and different capacities for mechanical deformation (Mao, 2002; Mao et al., 2003; Radhakrishnan and Mao, 2004). In addition, sutural tissues and structures have been shown to change over time in humans and laboratory animals. For example, connective tissue cells and fibers in sutures progressively decrease in concentration, and collagen increases in tensile strength while decreasing in extensibility (Gross, 1961; Milch, 1966). In human faces, the overall structure of sutures becomes increasingly irregular, if not fused, with advancing age. This occurs due to the formation of bony projections or interdigitations at the sutural bony surface (Masseler and Schour, 1951; Kokick, 1976; Miroue and Rosenberg, 1975).

In vivo work using a mouse model demonstrates osteoid bone formation along these convex interdigitations (i.e., the convex bone front; Byron et al., 2004), and osteoclast resorption along concave interdigitations (i.e. the concave bone front; Byron, 2006). The iteration of these processes is responsible for cranial suture waveform patterning. Increases in the complexity of this pattern in mice are accompanied by increases in masticatory muscle function and suture extensibility (Byron et al., 2004; Byron et al., 2006a). Among the primates known to differentially exploit materially tough food items such as *Cebus apella*, increased cranial suture complexity is observed when compared to other congenerics that do not exploit such obdurate foods (Byron et al., 2006b). Thus it is proposed that mechanical information concerning mastication manifests itself, in part, through suture morphology.

Sutures clearly have an important influence on the strain distribution throughout the skull, but our understanding of the impact of sutures is incomplete. Some of the difficulties in attempting to address strain in and around craniofacial sutures in the studies of living primates can be resolved using an in vitro approach. In vitro

methods have been used in biomechanical research for assessing deformation patterns of mandibles (Daegling and Hylander, 1998; Daegling and Hotzman, 2003), and in clinical and biomedical research for assessing the effects that prosthetic instruments have on bone surface strains (Yamashita et al., 2006; Dechow and Wang, 2006). In vitro experiments on cadavers allow loads and boundary conditions to be controlled (Marinescu et al., 2005); sites normally difficult to access can be measured and the sutural morphology (patent, fused, or degree of interdigitation) can be better evaluated; measurements at various points under identical loading and boundary conditions can provide a synchronous global strain pattern; and comparisons of the results of finite element analyses (FEA) to in vitro studies (in conjunction with comparisons to in vivo studies) permit validation of finite element (FE) models (Richmond et al., 2005).

Given the benefits of such an approach, we developed techniques for careful measurement and analysis of in vitro strain in primate skulls on bony surfaces and across sutures. In this paper, we introduce our design for in vitro experiments, and the reliability of our methods. We explore the strain patterns on the macaque facial skeleton during in vitro loading, and compare the results on bone with that found across several facial sutures.

The influence of sutures on strain patterns also holds important implications for the attempts to investigate strain distributions throughout the craniofacial skeleton, including FEA of craniofacial biomechanics (e.g., Strait et al., 2005; Richmond et al., 2005). Finite element analysis, which enables the examination of how objects of complex design deform and resist loads using advanced computational and engineering techniques, has become one of the most promising tools in the study of functional morphology, especially of the craniofacial skeleton in human and nonhuman primates (Richmond et al., 2005).

This study uses an in vitro model to explore the distribution of strain throughout the macaque craniofacial skeleton, with special focus on the influence of sutures.

8.2 Materials and Methods

8.2.1 Materials and Specimen Handling

One fresh head of a male long-tailed or crab-eating macaque (*Macaca fascicularis*), age 9.5 years, was used in this test. All permanent teeth including the third molars were in situ. Cause of death was not related to primary bone diseases. Animal's tissue use conformed to all NIH, state, and federal standards.

In order to prevent changes in bone material properties, special considerations were made concerning dehydration and temperature. Dehydration will increase bone stiffness but decrease bone strength (Evans and Lebow, 1951). In order to prevent dehydration, all soft tissues were kept on the head, except in the nuchal area where all muscles were removed. The posterior temporalis muscles on both the right and left sides of the skull were lifted with a periosteal elevator, in order to expose the

underlying bony surface for stabilization. The head was wrapped with paper towels soaked in isotonic saline during the mounting process and during tests. Mechanical tests of bone material properties are also influenced by surrounding temperatures. For example, experiments at room temperature (23°C) produced 2–3% percent higher elastic moduli than the bone tested at 37°C (Bonfield and Li, 1966). The specimen was normally tested at a room temperature of 19°C.

8.2.2 Stabilization of the Head

The back of the head was fixed to orthodontic stone, and the latter was tightly fixed to an apparatus consisting of cross-slides and a rotary table (Sherline Products, Vista, CA), which permitted rotational and three-dimensional linear adjustments for proper positioning (Fig. 8.1).

8.2.3 Loading Forces and Loading Rate

Loads were applied by using a screw-driven DDL RT200 loading machine (Test Resources, Inc., Shakopee, MN, USA). The loading was normal to the functional occlusal plane (FOP), defined by the cusps of the second molar (M^2) and the third premolar (PM^3) (Thayers, 1990). Previous studies have measured voluntary bite forces in three adult female *M. fascicularis* on the second and third molars (Hylander, 1979). The average bite forces are less than 10 kg or 98 Newtons (N),

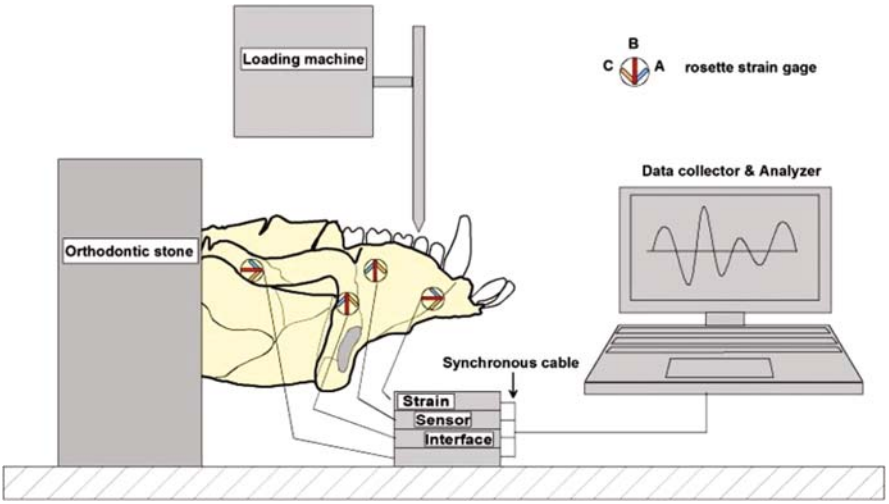

Fig. 8.1 Experiment setup. The head was fixed posterior to the external acoustic meatus using orthodontic stone, which was further fixed to an apparatus consisting of cross-slides and a rotary table

and the largest bite force is approximately 37 kg or 363 N (Hylander, 1979). The loads of 130 N were applied to the central incisor. Higher loads of 260 N were placed on the central fossa of the third molar, because in monkeys, maximum molar biting force is 2–2.5 times higher than maximum incisor biting force, based on the estimates derived from jaw geometry (Dechow and Carlson, 1990). Loads of 195 N (average of the former two) were placed on the buccal cusp of the fourth premolar. The resulting loads and displacements were recorded on computer directly via the software program MTestWR Windows (MTWR) (50 Hz). The loading speed was constant in all loading events. The loading rate was 10 N/s, and the highest strain rate on bone surfaces was 95 με/s, but most experiments exhibited strain rates lower than 20 με/s. The loading was immediately cancelled when the desired "bite force" was reached.

8.2.4 Strain Gage Measurements

Surface bone and suture strains were measured during artificial loadings by using small (Diameter 4 mm) 3-element rosette (45°) strain gages (UFRA-1-11-3LT; Tokyo Sokki Kenkyujo, Tokyo, Japan). After reflecting the overlying tissues, the periosteum at the gage site was incised and reflected. The exposed bone was cleaned with 100% acetone. The gage was affixed with Loctite cyanoacrylate. Gages were put on the right side of the head. Locations and orientations of the B-element of 26 gages are detailed in Table 8.1. Twenty-six strain gages were placed across the external surface of the facial skeleton, including hard palate, zygomatic arch, internal orbital wall, circumorbital area, alveolar area, and midface (Table 8.1; Fig. 8.2). Seven gages were put on six patent or fused sutures, including zygomatico-temporal, zygomatico-frontal, maxillo-zygomatic suture, premaxillo-maxillary, anterior midpalatal, and transpalatal. The mid-and transpalatal sutures and the inferior half of the premaxillo-maxillary suture were fused, all others were patent or open. On the bone surface, the B-element was placed along the long axis of bone, which was defined locally (see details in Table 8.1). When a gage was placed on a suture, the B-element was aligned perpendicular to the primary orientation of the suture. Periosteum was lifted regionally for applying strain gages. After the attachment of strain gages, the periosteum was flapped back and the skull was wrapped with paper towels soaked in isotonic saline.

At least five cycles of loading were applied on each loading location on the right side (i.e., gage side) and left side (i.e., non-gage side), respectively. During loading, strains were measured by four synchronized PCD-300A Sensor Interface (Kyowa Electronic Instruments, Tokyo, Japan), and strain measurements were directly stored in a computer (Sampling rate: 100 Hz). Each PCD-300A has four channels (16 channels in total), allowing simultaneous data collection from five rosette gages (i.e., 15 channels). The remaining channel was occupied by a single-element gage placed on the infraorbital area. This gage was used to monitor and calculate the variation in strains for the same loading regime when collecting data from different

Table 8.1 Strain gage sites, orientations, and descriptions

Gage number	Gage site code	Gage site	Orientation of the B-element
1	Parch	posterior zygomatic arch	along the axis of arch
2	Zts	zygomatico-temporal suture	normal to the suture
3	Marh	anterior zygomatico arch	along the axis of arch
4	aarch	zygomatic bone anterior to zygomatic arch	sup. – inf.
5	zfp	frontal process of zygomatic bone	along axis of process
6	zfs	zygomatico-frontal suture	normal to the suture
7	msot	median supraorbital torus	sup. – inf.
8	rio	Rostral interorbital area	sup. – inf.
9	mfp	lower part of the frontal process of the maxillary bone	sup. – inf.
10	pmmss	premaxillo-maxillary suture, superior part	normal to the suture
11	mlp	maxillary bone lateral to the piriform	sup. – inf.
12	prem	premaxillary bone, above the area between I^1 and I^2	sup. – inf.
13	pmmsi	premaxillo-maxillary suture, inferior part	normal to the suture
14	alc	alveolus above canine	sup. – inf.
15	alp	alveolus above PM^4	sup. – inf.
16	alm	alveolus above M^2	sup. – inf.
17	mbc	Center of maxillary bone body	sup. – inf.
18	mzs	maxillo-zygomatical suture	normal to the suture
19	zbi	inferior zygomatic bone	med. – lat.
20	orbwm	medial orbital wall	ant. – post.
21	orbws	superior orbital wall	ant. – post.
22	orbwl	Lateral orbital wall	ant. – post.
23	mps	midpalatal suture anterior to the transpalatal suture	normal to the suture
24	apm	anterior palatine process of maxilla, between C^1 and PM^3	ant. – post.
25	tps	transpalatal suture	normal to the suture
26	phpp	oral surface of horizontal plate of palatine bone	ant. – post.

Abbreviations: I^1 – central incisor; I^2 – lateral incisor; C^1 – canine; PM^3– third premolar; PM^4– fourth premolar; M^2– second molar

gage groupings. The error in positioning for same loading regime was less than 6.3%. Thus global bone and suture behavior during in vitro tests can be summed with confidence from the experiments of different gage groupings using the same loading regime.

8.2.5 Data Analysis

Tensile (ε_1, positive in definition) and compressive (ε_2, negative in definition) strains and the orientation of tensile strain (ε_1°) were calculated by using the strain data analyzer program software DAS-100A (Kyowa Electronic Instruments, Tokyo,

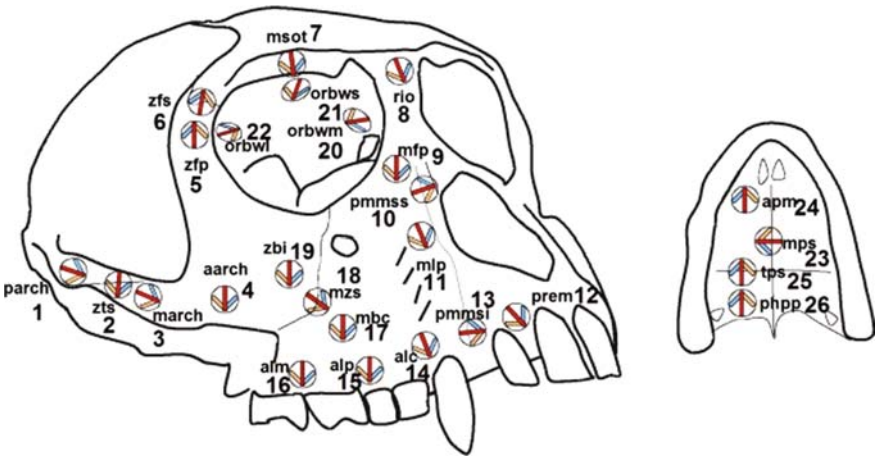

Fig. 8.2 Twenty-six gage sites. The orientation of B-element, the darkened central sensor of the gage, was assigned based on local skeletal morphology. Gages No. 1–3 were on the zygomatic arch. Gage No. 4 was in the lower part of the body of the zygomatic bone. Gages No. 5–7 were in the circumorbital area formed by the supraorbital torus, and the anterior surface of the lateral wall formed by the frontal process of the zygomatic bone and the zygomatic process of the frontal bones. Gage No. 8 was on the glabella area. Gages No. 9–11 was on the anterior middle face. Gages No. 12–16 were on the alveolar area, the alveolar profess of the maxillary and premaxillary bones. Gages No. 17–19 were on the middle part of middle face. Gages No. 20–22 inside the orbit were on the medial, lateral, and superior orbital walls. Gages No. 23–24 were on the oral roof. There were six patent sutural sites, including Site 2 on the zygomatico-temporal suture, Site 6 on the zygomatico-frontal suture, Site 10 on the superior premaxillo-maxillary suture, Site 18 on the maxillo-zygomatic suture, Site 23 on the intermaxillary suture, and Site 25 on the maxillio-palatine suture in the palatal area. Besides, Site 13 was put on the fused inferior section of the premaxillo-maxillary suture

Japan). The orientations of ε_1 were ultimately calculated in degrees relative to the B-element of each gage to indicate their relationships with the anatomical features of the skull (Table 8.1). Descriptive statistics, including means and standard deviation, were calculated for all measurements using Minitab statistical analysis program (MINITAB 14; Minitab, State College, PA). Circular descriptive statistics including angular means, circular standard deviation, and a Rayleigh's test of uniformity (Zar, 1999) were calculated with the Oriana Circular Statistical Analysis Program 2.02 (Kovach Computing Services, Wales, UK). Paired sample t-tests and paired circular sample tests (Hotelling test) (Zar, 1999) were used to assess the differences in strain patterns (tensile, compressive and shear strains, strains modes, and strain orientations) between repeated loadings, between gage-side and non-gage side loadings, and between sites at two sides of sutures ($\alpha = 0.05$). Paired data here refer to the analysis of tabulated pairs. For example, strain measurements on a site of two different experiments, or same strain parameters (i.e., strain magnitudes, modes, or orientations) of two different sites during the same loading experiments could be viewed as a paired data.

8.3 Results

8.3.1 Reliability of In Vitro Strain Measurements

The reliability of strain measurements was assessed by repeated loadings. Paired sample tests showed that there were no significant differences at all gage sites between paired mean (1) shear strains, and (2) strain modes (absolute value of the ratio between tensile and compressive strains). Nor were there any significant differences in the angle of principal strains according to Hotelling tests. For example, between two tests with a loading of 130 N placed on the right central incisor, the difference in 26 paired angles was $\pm$ 6.7°, which was not significant (Hotelling test: $F = 0.25$, $0.975 < P < 0.999$). Theoretically, the variance of surface suture and bone strain would be due solely to the methodological error since only a single skull was loaded under invariant conditions. The grand mean of the coefficient of variation of maximum tensile and compressive strains of 26 gage sites in all six experiments was 7.8%, suggesting an error of $\pm$7.8%, or an overall precision level of 92.2% (Here the precision was defined as 1 minus CV).

8.3.2 Strain Patterns

Over all, at both bone surface and sutural sites, with increasing loading forces, the strain magnitudes increased gradually. However, the strain mode (ratio between tensile strain and compressive strain) and the orientation of the tensile strain remained constant (Fig. 8.3). For example, during the application of a load of 130 N was placed on the gage-side central incisor, both tensile and compressive strains at the posterior zygomatic arch (Site 1) were increasing in magnitude. The ratio between the tensile and compressive strains was constantly around 3.4. The orientation of the tensile strain was approximately about 80.9° in relation to Element B (Table 8.2). At the neighboring suture site, Site 2 on the zygomatico-temporal suture, the same phenomenon was observed (Fig. 8.3b). This site had strain about six times higher than the adjacent bone surface. During the loading process, similar to the bone surface site, the strain pattern remained constant except for the change in strain magnitude, the orientation of tensile strain was consistently around 21° to Element B. Curiously, the increase of strain magnitude across the sutures was more consistent than that on the bone surface, which might be related to different material structures and properties as well as bone and sutural tissues (Fig. 8.3).

Differences in strain pattern between the bone surfaces and the sutures were found during the period of post-loading. On the suture, the strains did not disappear totally: there were always residual strains in the sutures, indicating a viscoelastic response, if not plastic deformation. The residual tensile strain was 60 $\mu\varepsilon$ at an angle of $-26.6°$ to Element A, and was 40 $\mu\varepsilon$ in compression (Fig. 8.3b).

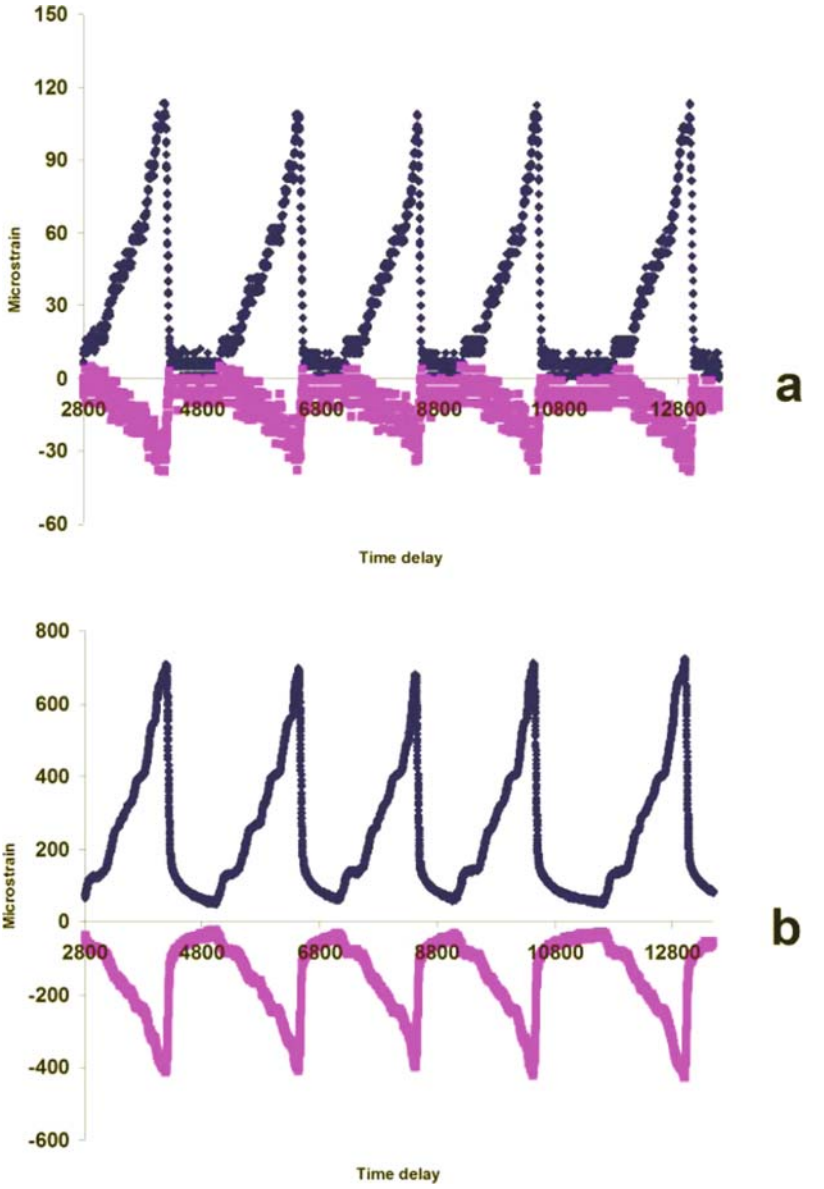

Fig. 8.3 Real-time strain records at a bone surface site, the posterior zygomatic arch (Gage Site No. 1) (**a**), and at a sutural site, the zygomatico-temporal suture (Gage Site No. 2) (**b**), during 130 N load on the gage-side central incisor. The positive values were tensile strains; the negative values were compressive strains. Notice the strain magnitudes were remarkably higher on the sutures than on the adjacent bone surface. With increasing loading forces, the strain magnitudes increased gradually. After the canceling of loads, there were always residual strains in the sutures (**a**), indicating a viscoelastic response. Conceivably, there should be residual strains on the bone surface, but this situation was not clearly demonstrated here (**b**)

Table 8.2 In vitro strain measurements when a load of 130 N was placed on right and left central incisors ($N = 5$)

130 N on right central incisor (gage side)										
	Tension (ε_1)		Compression (ε_2)		Shear ($\gamma = \varepsilon_1 + \lvert\varepsilon_2\rvert$)		Mode ($\varepsilon_1/\lvert\varepsilon_2\rvert$)		Orientation(ε_1°)	
Gage site	Mean	S.D.	Mean	S.D.	Mean	S.D.	Mean	S.D.	Mean	S.D.
1	108.5	3.0	−32.5	3.8	141.1	6.5	3.4	0.3	80.9	0.5
2	669.3	29.0	−386.3	21.9	1055.6	50.8	1.7	0.0	20.7	0.3
3	14.3	2.4	−45.3	1.7	59.6	3.6	0.3	0.0	20.5	1.6
4	200.2	3.7	−106.2	14.8	306.4	15.6	1.9	0.3	98.2	0.7
5	61.1	2.3	−71.1	2.3	132.2	4.7	0.9	0.0	98.8	0.3
6	268.4	6.5	−829.4	26.8	1097.9	33.2	0.3	0.0	28.9	0.2
7	88.9	2.4	−66.9	3.2	155.7	5.2	1.3	0.0	55.1	0.9
8	12.8	10.7	−175.8	8.4	188.7	7.2	0.1	0.1	69.7	0.7
9	61.7	7.4	−246.7	12.9	308.4	19.7	0.3	0.0	4.1	0.1
10	583.0	6.3	−973.0	8.2	1555.9	14.2	0.6	0.0	75.2	0.1
11	50.8	7.0	−180.2	8.3	231.0	14.3	0.3	0.0	21.6	5.0
12	925.4	8.8	−1211.4	13.4	2136.8	10.2	0.8	0.0	10.5	0.1
13	487.6	7.6	−315.6	1.9	803.2	8.7	1.5	0.0	9.4	0.1
14	237.9	4.0	−177.9	2.0	415.8	5.4	1.3	0.0	50.5	0.2
15	195.4	1.2	−76.4	0.8	271.8	0.4	2.6	0.0	71.8	0.3
16	121.6	2.0	−41.6	2.0	163.1	4.1	2.9	0.1	16.8	0.5
17	180.0	6.9	−86.0	4.8	266.0	10.3	2.1	0.1	85.0	0.4
18	354.4	2.6	−871.4	8.4	1225.7	7.7	0.4	0.0	88.1	0.2
19	147.7	3.6	−102.7	2.6	250.4	5.3	1.4	0.0	70.6	0.6
20	119.7	2.4	−504.7	5.3	624.4	7.6	0.2	0.0	12.2	0.2
21	190.3	4.4	−256.3	3.4	446.6	6.9	0.7	0.0	75.7	0.4
22	132.3	3.6	−162.3	3.8	294.6	3.7	0.8	0.0	25.7	0.3
23	346.6	2.7	−348.6	3.0	695.2	2.8	1.0	0.0	31.2	0.4
24	263.0	5.4	−176.0	5.4	439.0	10.0	1.5	0.0	14.1	0.7
25	253.3	2.9	−74.3	4.8	327.5	2.8	3.4	0.3	24.5	0.6
26	216.4	4.0	−42.4	2.8	258.8	6.7	5.1	0.2	14.6	0.2

Table 8.2 (continued)

130 N on left central incisor (non-gage side)										
	Tension (ε_1)		Compression (ε_2)		Shear ($\gamma = \varepsilon_1 + \lvert\varepsilon_2\rvert$)		Mode ($\varepsilon_1/\lvert\varepsilon_2\rvert$)		Orientation(ε_1°)	
Gage site	Mean	S.D.	Mean	S.D.	Mean	S.D.	Mean	S.D.	Mean	S.D.
1	158.1	2.0	−49.1	3.1	207.3	3.7	3.2	0.2	77.9	0.5
2	875.5	11.4	−395.5	12.6	1270.9	23.6	2.2	0.0	20.3	0.5
3	27.2	2.1	−103.2	2.0	130.4	3.6	0.3	0.0	10.3	0.6
4	201.0	3.7	−97.0	8.5	298.0	11.0	2.1	0.2	101.0	0.7
5	67.1	2.5	−61.1	2.0	128.2	4.0	1.1	0.0	178.7	0.4
6	187.6	3.7	−526.6	5.3	714.2	8.3	0.4	0.0	31.7	0.2
7	68.4	0.6	−38.4	3.0	106.8	2.9	1.8	0.1	56.6	1.8
8	7.7	5.3	−141.7	6.7	149.4	7.6	0.1	0.0	63.9	1.3
9	81.5	7.3	−266.5	16.3	348.0	19.6	0.3	0.0	2.9	0.1
10	436.1	11.0	−810.1	14.3	1246.2	24.9	0.5	0.0	74.2	0.1
11	62.4	23.2	−229.4	17.2	291.9	9.3	0.3	0.1	56.4	0.7
12	298.8	16.2	−202.8	13.8	501.6	29.2	1.5	0.0	80.8	0.3
13	9.3	3.5	−99.3	5.0	108.5	4.8	0.1	0.0	30.1	1.3
14	169.5	10.2	−77.5	3.9	247.1	13.8	2.2	0.1	47.6	0.8
15	93.4	8.5	−26.4	3.6	119.9	12.0	3.6	0.2	63.7	0.8
16	62.1	4.0	−6.1	2.0	68.2	5.9	10.8	1.9	88.2	0.9
17	132.1	2.9	−72.1	2.9	204.2	5.7	1.8	0.0	5.7	1.3
18	205.4	4.9	−110.4	43.1	315.8	47.1	2.3	1.1	76.7	2.7
19	120.2	3.3	−63.2	4.6	183.3	7.7	1.9	0.1	70.2	1.0
20	155.5	2.8	−530.5	8.4	686.0	10.8	0.3	0.0	11.5	0.1
21	141.6	4.3	−232.6	5.7	374.3	8.2	0.6	0.0	74.8	0.3
22	41.1	18.3	−189.1	15.9	230.2	5.4	0.2	0.1	25.3	0.4
23	263.9	2.8	−216.9	0.4	480.8	3.2	1.2	0.0	10.8	0.1
24	209.6	3.9	−372.6	3.7	582.2	6.5	0.6	0.0	87.0	0.1
25	253.2	3.7	−81.2	1.9	334.4	4.4	3.1	0.1	4.6	0.2
26	195.0	2.1	−45.0	2.1	240.0	2.9	4.3	0.2	20.0	0.5

8.3.3 Global In Vitro Facial Strain Field

Tables 8.2–8.4 summarize means and standard deviations for in vitro strain variables, including tensile strains (ε_1), compressive strains (ε_2), shear strains (γ), strain modes ($\varepsilon_1/|\varepsilon_2|$), and orientation of tensile strains (ε_1°). All mean angles of the tensile strains were significantly uniform in orientation (Rayleigh's test: $P < 0.001$), which means the orientation of strains at any specific sites were constant during identical loading regimes. Figures 8.4–8.6 illustrate the shear strain for each location under different loading conditions.

The loadings ipsilateral to the gages produced higher strains than the loads contralateral to the gages, especially when the loadings were placed on the posterior teeth, indicating various combinations of bending and twisting moments in the facial skeleton. When the central incisors and premolars were loaded, the principal strains suggested bending in the sagittal plane. The orientations of the maximum principal strains on the facial bone surfaces at 21 sites were comparable between the left and the right loadings on the incisors (Hotelling test: Incisor loadings, $F = 0.12$, $P = 0.99$; premolar loadings, ($F = 0.18$, $P = 0.97$). The differences in orientation between loadings on left and right molars were greater ($F = 2.184$, $0.10 < P < 0.25$), suggesting the presence of a strong torsional component during molar loading.

Theoretically, sites located in the median sagittal plane of the skull should have similar strain magnitudes when identical loadings are applied symmetrically. However, marked asymmetry was recorded. For example, when loadings of 130 N were put on the right and left central incisors respectively, the difference between the two resulting maximum shear strains was 21% at the glabella area (Site 8), and 31% at the midpalatal suture (Site 23), two sites located in the sagittal midline (Tables 8.3–8.4, Fig. 8.5). This might be explained by the asymmetry of the facial skeleton in the skull that was studied, or in the experimental rig.

Strain magnitudes demonstrate strain gradients related to the distance to the loading positions as seen in in vivo tests (i.e., Hylander and Johnson, 1997; Ross and Metzger, 2004). For example, when a loading of 130 N was placed on the gage-side central incisor, along the alveolar process, the mean shear values decreased significantly from 2136.8 $\mu\varepsilon$ at Site 12 (prem), to 803.2 $\mu\varepsilon$ at Site 13 (pmmsi), to 415.8 $\mu\varepsilon$ at Site 14 (alc), to 271.8 $\mu\varepsilon$ at Site 15 (alp), and to 163.1 $\mu\varepsilon$ at Site 16 (alm) (Table 8.2, Fig. 8.3).

8.3.4 Effect of Patent and Fused Sutures

Results showed that average strain values in patent sutures were remarkably higher than in adjacent regions of cortical bone (Tables 8.2–8.4, Figs. 8.4–8.6). For example, during the application of a load of 130 N on the gage-side central incisor, on five patent sutural sites on the face (Sites 2, 6, 12, and 18), the strain magnitude was on average about 7.2 times higher than that on the adjacent bone surface sites. Strain modes differed as well. Strain orientations were often considerably different on the cortical bone found on adjacent sides of patent sutures. For example, in all

Table 8.3 In vitro strains measurements when a load of 195 N was placed on right and left fourth premolars ($N = 5$)

195N on right fourth premolar (gage side)										
	Tension (ε_1)		Compression (ε_2)		Shear ($\gamma = \varepsilon_1 + \lvert\varepsilon_2\rvert$)		Mode ($\varepsilon_1/\lvert\varepsilon_2\rvert$)		Orientation (ε_1°)	
Gage site	Mean	S.D.	Mean	S.D.	Mean	S.D.	Mean	S.D.	Mean	S.D.
1	101.8	2.8	−29.8	5.0	131.6	5.4	3.5	0.6	14.1	0.7
2	772.0	15.3	−789.0	16.1	1561.1	29.7	1.0	0.0	29.6	0.3
3	58.0	1.3	−17.0	2.9	75.0	2.4	3.5	0.6	59.8	2.1
4	249.9	42.6	−321.9	29.7	571.7	63.3	0.8	0.1	172.9	1.8
5	122.6	3.1	−173.6	5.5	296.1	8.1	0.7	0.0	144.8	0.6
6	723.3	57.5	−2692.3	165.8	3415.7	223.2	0.3	0.0	13.1	1.5
7	108.5	5.3	−111.5	5.8	220.0	10.9	1.0	0.0	52.3	0.5
8	148.2	12.7	−185.2	19.2	333.5	27.1	0.8	0.1	77.4	1.0
9	65.1	8.6	−225.1	21.3	291.2	26.8	0.3	0.0	89.8	0.1
10	370.0	11.5	−391.0	12.0	760.9	22.6	0.9	0.0	79.6	0.2
11	207.2	6.0	−167.2	8.0	374.5	10.9	1.2	0.1	41.9	1.2
12	95.0	5.9	−14.0	1.6	109.0	5.7	6.9	1.1	21.8	0.9
13	99.3	3.6	−80.3	4.4	179.7	7.8	1.2	0.0	80.1	0.4
14	477.5	20.8	−177.5	5.7	655.0	26.4	2.7	0.0	65.5	0.3
15	405.5	8.0	−1541.5	39.1	1947.0	46.7	0.3	0.0	33.1	0.5
16	451.8	18.6	−410.8	15.0	862.7	33.6	1.1	0.0	35.8	0.1
17	259.8	28.0	−912.8	44.9	1172.5	59.0	0.3	0.0	86	0.4
18	716.0	20.5	−1332.0	67.7	2048.0	84.6	0.5	0.0	88.3	0.5
19	178.9	16.7	−136.9	14.2	315.8	28.2	1.3	0.1	78.8	0.7
20	132.3	2.4	−352.3	5.1	484.6	7.3	0.4	0.0	1.4	0.2
21	366.2	6.5	−368.2	8.1	734.3	14.5	1.0	0.0	78.7	0.2
22	206.5	8.5	−403.5	7.0	610.1	9.8	0.5	0.0	36.8	0.2
23	280.5	21.7	−242.5	9.7	522.9	28.6	1.2	0.1	50.8	0.5
24	30.5	2.7	−132.6	7.4	163.1	7.6	0.2	0.0	50.3	1.8
25	230.7	16.1	−221.7	10.3	452.4	25.8	1.0	0.0	52	0.3
26	79.0	4.7	−34.0	5.7	113.0	7.7	2.4	0.4	7.4	1.8

Table 8.3 (continued)

195 N on left fourth premolar (non-gage side)

	Tension (ε_1)		Compression (ε_2)		Shear ($\gamma = \varepsilon_1 + \lvert\varepsilon_2\rvert$)		Mode ($\varepsilon_1/\lvert\varepsilon_2\rvert$)		Orientation (ε_1°)	
Gage site	Mean	S.D.	Mean	S.D.	Mean	S.D.	Mean	S.D.	Mean	S.D.
1	113.3	4.0	−25.3	2.0	138.5	5.9	4.5	0.3	84.6	0.7
2	699.1	27.3	−402.1	14.8	1101.2	40.6	1.7	0.0	26.5	0.5
3	23.9	3.8	−69.9	5.3	93.7	8.5	0.3	0.0	8.1	1.1
4	117.0	14.3	−55.0	7.9	172.0	22.1	2.1	0.1	169.5	2.0
5	43.5	7.0	−27.5	3.5	71.1	10.4	1.6	0.1	159.5	1.8
6	447.9	29.0	−192.9	16.7	640.7	45.5	2.3	0.1	81.9	0.7
7	47.5	3.5	−9.5	2.5	57.0	3.4	5.5	1.9	54.3	1.5
8	4.1	2.7	−158.7	20.4	162.7	20.2	0.0	0.0	10.8	1.4
9	58.2	7.3	−222.2	13.2	280.4	20.0	0.3	0.0	68.6	1.1
10	27.1	2.8	−341.1	17.3	368.2	20.1	0.1	0.0	50.1	0.9
11	30.9	5.6	−47.9	3.6	78.8	3.6	0.7	0.2	59	3.3
12	3.0	3.7	−22.3	4.0	25.4	6.1	0.1	0.1	49.1	6.8
13	5.4	3.2	−39.8	6.6	45.1	6.5	0.1	0.1	11.5	4.4
14	33.2	7.5	−7.2	2.5	40.4	8.5	5.1	1.9	46.6	2.4
15	21.9	4.6	−20.9	4.7	42.7	4.9	1.2	0.6	59.7	2.8
16	35.7	3.2	−44.7	10.1	80.3	12.6	0.8	0.2	40.5	2.3
17	58.7	6.4	−10.6	9.4	69.4	5.6	14.8	12.1	12.8	4.7
18	333.6	48.7	−27.4	19.4	361.0	35.7	44.9	54.4	12.3	2.5
19	65.2	8.0	−11.2	2.3	76.5	8.6	6.0	1.4	74.8	2.6
20	205.8	9.0	−488.8	21.3	694.6	30.2	0.4	0.0	15.9	0.2
21	113.6	6.0	−194.6	3.6	308.2	7.4	0.6	0.0	2.5	0.4
22	127.9	3.5	−77.9	8.1	205.9	10.8	1.7	0.2	41.3	1.4
23	133.0	10.2	−29.0	3.3	161.9	8.6	4.7	0.8	36	0.6
24	119.1	4.9	−28.9	8.0	148.0	12.5	4.4	1.1	88.7	0.6
25	210.4	8.2	−16.4	2.2	226.7	7.7	13.1	1.7	43	1.1
26	108.5	6.7	−43.5	8.7	152.0	3.7	2.6	0.7	86.8	0.5

Table 8.4 In vitro strains measurements when a load of 260 N was placed on right and left third molars (N=5)

	260 N on right third molar (gage side)									
	Tension (ε_1)		Compression (ε_2)		Shear ($\gamma=\varepsilon_1+\lvert\varepsilon_2\rvert$)		Mode ($\varepsilon_1/\lvert\varepsilon_2\rvert$)		Orientation (ε_1°)	
Gage site	Mean	S.D.	Mean	S.D.	Mean	S.D.	Mean	S.D.	Mean	S.D.
1	88.5	3.4	−185.5	16.7	274.0	17.5	0.5	0.0	62.8	0.9
2	29.3	10.7	−1329.5	85.8	1358.8	92.1	0.0	0.0	5.1	1.3
3	101.3	6.8	−31.3	6.2	132.6	12.2	3.3	0.5	53.4	6.0
4	111.1	13.8	−294.1	16.8	405.3	22.3	0.4	0.1	149.2	2.2
5	88.0	5.3	−61.0	3.9	149.0	9.0	1.4	0.0	144.2	1.9
6	634.7	45.4	−2717.7	119.8	3352.4	164.9	0.2	0.0	9.7	0.5
7	55.5	4.1	−113.5	8.5	169.0	6.5	0.5	0.1	63.2	1.3
8	192.3	2.5	−36.3	6.0	228.6	7.1	5.4	0.8	88	0.7
9	69.6	4.5	−261.6	12.6	331.1	16.4	0.3	0.0	68	0.9
10	19.4	2.1	−27.4	5.4	46.8	7.2	0.7	0.1	46.8	4.7
11	25.8	5.8	−29.8	6.1	55.7	6.2	0.9	0.3	22	13.1
12	39.1	4.8	−16.1	0.5	55.2	4.5	2.4	0.4	82	2.0
13	48.6	2.8	−47.6	2.8	96.2	4.3	1.0	0.1	58.9	0.4
14	30.6	3.5	−93.6	2.4	124.2	3.3	0.3	0.0	53.2	1.3
15	90.8	3.1	−96.8	3.7	187.6	6.5	0.9	0.0	41.3	0.4
16	294.8	18.7	−184.8	9.4	479.5	27.9	1.6	0.0	35.3	0.2
17	48.2	13.3	−131.8	10.7	180.0	15.8	0.4	0.1	49.3	4.8
18	267.6	36.7	−332.6	54.4	600.1	90.5	0.8	0.0	83.1	1.5
19	110.3	5.6	−56.3	8.9	166.5	13.7	2.0	0.3	14.5	4.2
20	137.0	5.0	−212.0	9.8	349.0	14.5	0.6	0.0	83.1	0.3
21	399.3	15.6	−337.3	13.2	736.7	28.8	1.2	0.0	79.7	0.3
22	225.1	5.4	−405.1	12.2	630.1	17.5	0.6	0.0	44.4	0.2
23	15.4	13.8	−173.1	12.3	188.5	9.6	0.1	0.1	54.4	1.4
24	53.7	22.5	−193.3	8.7	247.0	30.1	0.3	0.1	61.5	3.9
25	33.1	10.9	−225.9	3.3	259.0	12.8	0.1	0.0	72.3	2.2
26	36.4	20.6	−215.2	27.6	251.6	12.9	0.2	0.1	49.4	3.6

Table 8.4 (continued)

260 N on left third molar (non-gage side)										
	Tension (ε_1)		Compression (ε_2)		Shear ($\gamma = \varepsilon_1 + \lvert\varepsilon_2\rvert$)		Mode ($\varepsilon_1/\lvert\varepsilon_2\rvert$)		Orientation (ε_1°)	
Gage site	Mean	S.D.	Mean	S.D.	Mean	S.D.	Mean	S.D.	Mean	S.D.
1	15.7	2.7	−24.7	4.2	40.4	4.0	0.7	0.2	51.4	4.0
2	34.3	14.5	−220.7	3.7	255.0	18.2	0.2	0.1	66.5	5.7
3	15.9	3.0	−2.4	1.2	18.2	4.1	0.0	0.0	36	18.0
4	55.6	2.3	−52.6	3.1	108.2	4.8	1.1	0.0	157	3.3
5	48.3	4.0	−25.3	2.2	73.5	5.1	1.9	0.2	172.5	0.6
6	291.0	15.4	−354.0	6.8	645.0	22.0	0.8	0.0	55.9	0.3
7	44.6	5.2	−16.6	3.8	61.3	2.8	2.9	1.0	58.8	3.4
8	110.3	9.1	−33.7	3.2	144.0	8.6	3.3	0.5	33.8	3.1
9	111.1	1.1	−125.1	16.8	236.2	17.1	0.9	0.1	50.2	3.7
10	9.9	3.9	−239.9	25.4	249.9	26.9	0.0	0.0	42.4	2.5
11	39.9	2.7	−12.9	3.1	52.7	2.9	3.4	1.1	36.9	11.5
12	8.8	2.7	−22.8	7.0	31.7	8.8	0.4	0.1	80.7	1.4
13	15.4	4.4	−38.4	4.1	53.8	6.1	0.4	0.1	4.8	0.9
14	32.2	1.7	−11.2	0.9	43.4	1.8	2.9	0.3	53.8	4.0
15	3.3	2.1	−20.5	4.3	23.8	5.4	0.2	0.1	22.9	5.2
16	41.3	1.7	−68.3	3.4	109.5	3.7	0.6	0.0	25.4	0.9
17	91.1	3.1	−49.9	4.5	141.0	3.7	1.8	0.2	57.2	4.9
18	241.9	13.1	−408.9	29.8	650.7	41.6	0.6	0.0	86.9	0.4
19	76.5	6.2	−40.5	2.3	116.9	7.3	1.9	0.2	71	1.1
20	101.2	2.1	−281.2	2.7	382.4	3.6	0.4	0.0	10.3	0.8
21	211.4	2.3	−212.4	4.1	423.9	5.5	1.0	0.0	7.6	0.6
22	62.3	7.2	−114.3	5.8	176.5	2.4	0.5	0.1	36.1	0.6
23	129.7	8.6	−286.7	17.5	416.4	12.1	0.5	0.1	47.3	0.6
24	121.9	10.8	−45.9	8.9	167.8	4.0	2.8	0.8	54.8	1.1
25	126.2	3.0	−30.2	9.6	156.4	12.2	4.6	1.5	81.8	0.7
26	15.8	12.0	−41.8	25.7	57.5	13.8	1.3	1.8	83.9	4.4

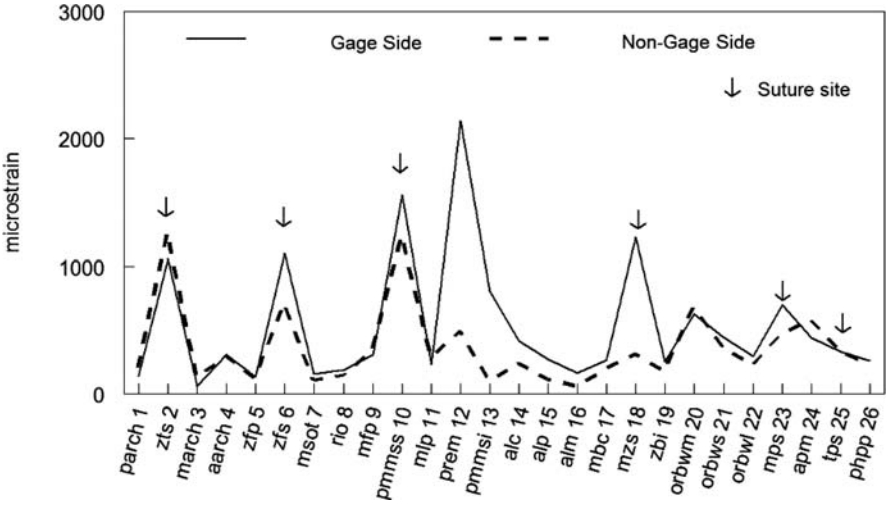

Fig. 8.4 Shear strain during 130 N load on central incisor. The solid line represents the result of gage-side loading experiments; the dashed line represents the result of non-gage side loading experiments. Gage sites were arranged from left to right following the sequence used in tables. Points of strain values were connected to form lines and peaks on the line corresponded to high strain values at sutural sites. Note the peaks at patent sutural sites including Site 2 (zygomatico-temporal suture), Site 6 (zygomatico-frontal suture), Site 10 (upper part of the premaxillo-maxillary suture), and Site 18 (maxillo-zygomatic suture). Note the strain gradients from Site 12 to Site 16. Site 13 was on fused part of the premaxillo-maxillary suture

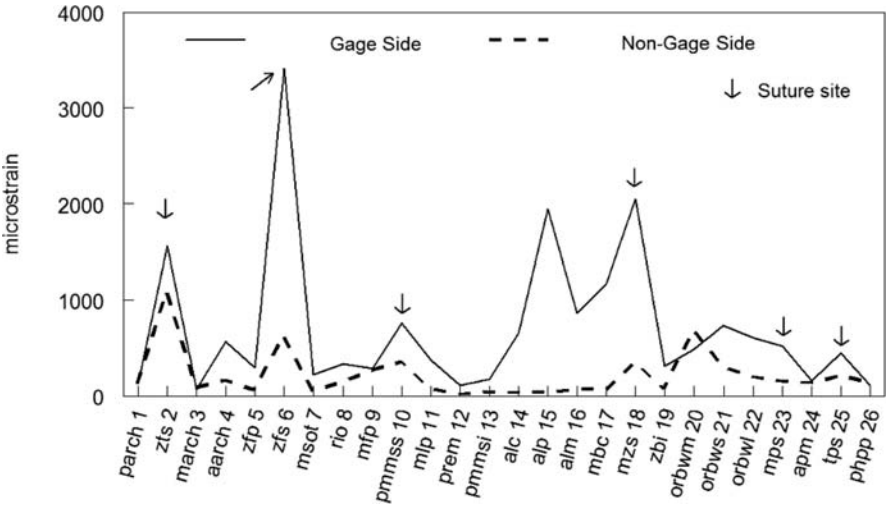

Fig. 8.5 Shear strain during 195 N load on fourth premolar. The solid line represents the result of gage-side loading experiments; the dashed line represents the result of non-gage side loading experiments. Note high strains on the facial sutural sites and on the alveolar process, Sites 14–16

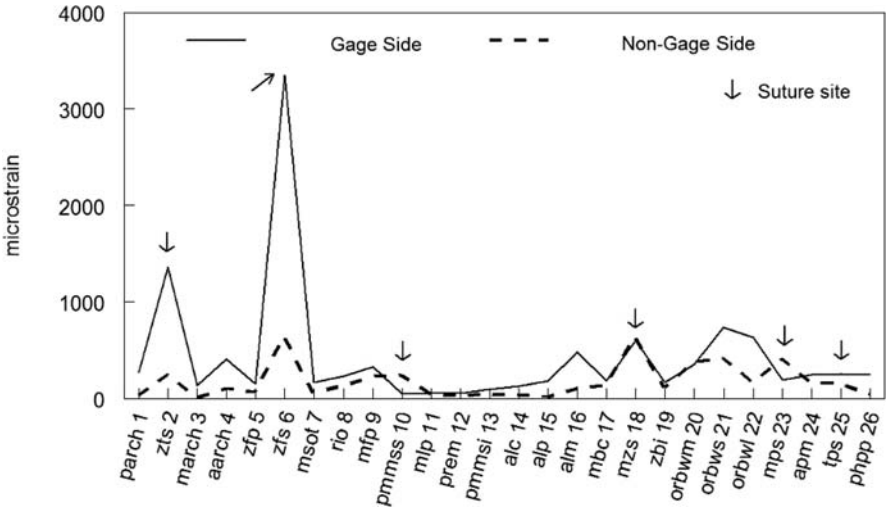

Fig. 8.6 Shear strain during 260 N load on third molar. The solid line represents the result of gage-side loading experiments; the dashed line represents the result of non-gage side loading experiments. Note high strains on two sutures at the posterior part of the face, Sites 2 and 6, but relatively low strains on other part of the facial skeleton

experiments, across the zygomatico-temporal suture and maxillo-zygomatic suture, the orientations of maximum principal strain changed significantly (Hotelling test: $F = 8.33$, $0.025 < P < 0.050$). Across fused sutural sections, such as the inferior part of the premaxillo-maxillary suture and the transverse palatal suture, the shear strains were comparable to the surrounding bone strains or compatible with a surrounding strain gradient. The fused sutures or sutural sections behaved mechanically like the bones around them.

The various sutures exhibit a range of mechanical behaviors during different loading regimes. The zygomatico-temporal sutures on the gage-side exhibited similar strain magnitudes during all incisor, premolar, and molar loading experiments. The zygomatico-frontal sutures differed under posterior tooth loading compared to other loading regimes. Other sutures also showed remarkable changes in strain magnitude with shifts in the point of loading. The facial sutures on the balancing side had smaller strains than on the loading side, similar to strains on the bone surface.

8.4 Discussion

8.4.1 Relevance of In Vitro Approaches to the Study of Functional Morphology

Global surface bone and sutural strains were measured using an in vitro method. The method was found to be reliable and provides the data necessary for the validation

of finite element models. Loading results demonstrate that the bending and twisting of the macaque facial skeleton, and the strain gradients on the bony surfaces, are generally comparable to the findings of in vivo experiments in pigs, although differing in detail (Rafferty et al., 2003). These results, in conjunction with in vivo studies (i.e., Hylander, 1986; Hylander et al., 1991; Daegling, 1993; Hylander and Johnson, 1997; Dechow and Hylander, 2000; Herring and Teng, 2000; Ravosa et al., 2000; Ross, 2001; Ross et al., 2002), can provide a baseline for validating FE models. For example, in vitro validation of FE models provides an assessment of how accurately geometry and material properties have been modeled under conditions in which loads and constraints can be tightly controlled. Once it has been established that geometry and material properties have been modeled well, then in vivo validation studies can assess how well loads and constraints have been modeled under conditions that are more physiologically realistic. Thus, a validation procedure that employs both in vitro and in vivo data allows an assessment of model validity that is more precise than one that employs in vivo data alone.

Physiological deformation of the craniofacial skeleton during mastication takes place due to a combination of forces at the teeth and the TMJ generated by the contraction of the masticatory muscles at their respective regions of attachment. In the in vitro tests presented here, the external loads and reaction forces are different. External loadings were put on a single tooth, and the posterior part of the skull was stabilized. The lack of loadings at muscle attachment sites would call into question any meaningful comparison between in vivo and in vitro deformations near muscle insertions. Such differences were obvious, especially in the zygomatic arch. Very high strains are generally exhibited in this region, both during in vivo experiments (Hylander et al., 1992; Hylander and Johnson, 1997) and in simulations with in vivo loading condition using FEA (Strait et al., 2005; Wright et al., in review). However, this lack of congruence near muscle insertion sites does not cast into doubt the fact that patterns of in vitro facial strains are essentially similar to in vivo facial strains.

It should be noted that while using in vitro data, the loading rates should be considered. The rate at which loading is applied during biomechanical experiments has an influence on the apparent stiffness of bone, as bone, like nearly all biological materials, is viscoelastic in its natural state (Lakes, 2001). When the loading speed is high, the strain will be increased by an order of magnitude, and measured bone strength will increase by about 15% (Carter and Hayes, 1977). In this analysis, as the loading speed is significantly slower than that in physiological conditions, it is reasonable to conclude that the in vitro bone strain is lower than in in vivo conditions if the loading regimes are identical.

The residual strains on the sutural sites are likely due to higher loading forces and longer loading durations in vitro. The increase in strain magnitude measured on the sutures was more consistent than on the bone surfaces when loads were increasing, which may relate to differences in the response of these tissues at low loading rates.

It is necessary here to remind readers that the in vitro tests are not equivalent to in vivo tests, and will never replace in vivo tests where the latter are feasible. There are some problems associated with in vitro experiments, such as changes in elastic properties of bone and sutural tissues postmortem, and using non-physiological

loading forces in terms of source and speed of loads. However, the magnitudes of these problems can be determined experimentally and adjustments can be made. An examination of the correspondence between in vitro and in vivo experiments with FE analyses that model crania with sutures will provide valuable information about how to interpret analysis of in vivo strains when experimental subjects have patent sutures. In vivo, in vitro, and FEA methods have different yet mutual-supporting merits for the common goal of discerning patterns of stain during biting and chewing.

8.4.2 Sutural Morphology and Functional Analysis of Craniofacial Skeletons

The in vitro experiments demonstrate the role of patent sutures in dampening cortical bone strain, a finding that is in agreement with previous in vivo studies. The orientations of the maximum principal strains often differed on either side of a suture, suggesting a redistribution of strain along with strain dampening. If sutures are considered fused when they are not, interpretation of the results of strain gage studies in a global scale and the use of these results for FE models might be biased. On the other hand, patterns of sutural closure could be of great importance for understanding craniofacial form and adaptation in primates, and the inclusion of sutures might enhance the precision of FE models and the accuracy of the study of functional morphology.

The effect of sutural fusion on patterns of stress and strain in the face needs further investigation. Ironically, the greatest chance of successfully measuring the impact of sutures lies with FEA, in which the patterns of sutural closure and the properties of sutures can be modeled. With accurate assignment of bone material properties, there is great improvement in the accuracy and precision of FE models (Strait et al., 2005). The inclusion of sutural morphology and sutural material properties, especially in the facial skeleton, where sutures often remain patent in adults, will further increase the accuracy of these models. As demonstrated here, this 9.5-year-old monkey, with a fully occluding dentition, still has a majority of patent sutures.

There is limited information in the literature on individual or global patterns of sutural closure in primates (Krogman, 1930; Chopra, 1957; Mooney and Siegel, 1991; Leigh and Shea, 1995; Falk et al., 1989; Hershkovitz et al., 1997; Brag, 1998; Wang et al., 2006b). This information is of great importance for modeling craniofacial biomechanics, and a systematic and applicable dataset has yet been established. Many questions still remain unanswered, such as: What are the patterns of fusion of all primary individual sutures? Are there species-specific patterns of sutural fusion? How does the fusion of sutures affect craniofacial growth and biomechanics? Our observations of various monkey skulls demonstrate different fusion patterns among functional areas, among different ontogenetic stages, and between the sexes (Wang et al., 2006b). We further postulated that sutural fusion patterns could be

species-specific. Given these findings and postulations, specific sutural morphology must be considered, along with species-specific skeletal elastic properties (e.g., Strait et al., 2005; Wang and Dechow, 2006; Wang et al., 2006c), when attempting to construct accurate FE models of particular species.

8.5 Conclusions

Global surface bone and sutural strains were measured using an in vitro method. This in vitro method was found to be a reliable approach for gleaning important, though non-physiological data, and can be easily modeled using Finite Element Analysis. The results of this experiment can also provide the data to validate FE models, besides in vivo or other strain measure experiments. Strain magnitudes and orientations were considerably different on the cortical bone adjacent to opposite sides of patent sutures. This pattern was generally not observed on either side of fused sutures. Considering sutures as fused when they are not may lead to biased interpretations of strain gage results and their extension to FEA. These findings demonstrate that in vitro experimental data, and information on sutural patency, may help to refine FE models, and increase our ability to understand anatomical function.

Acknowledgments This paper is dedicated to Dr. William L. Hylander, whose work on biomechanics and the function of primate skulls has provided inspiration for many researchers and has influenced a range of biomechanical and evolutionary projects, including this study. This research was supported by NSF-HOMINID grants to Q. Wang and C.D. Byron (BCS-0725183), P.C. Dechow (BCS-0725141), B.W. Wright (BCS-0725136), C.F. Ross (BCS-0725147), D.S. Strait (BCS-0725126), B.G. Richmond (BCS-0725122), and M.A. Spencer (BCS0725219). We thank Mr. Stanley Richardson for helping mount the monkey head for the loading tests. We also thank the editors Drs. Chris Vinyard, Matthew Ravosa, and Christine Wall, as well as two anonymous reviewers, for providing valuable advice for improving this manuscript.

References

Behrents, R.G., Carlson, D.S., and Abdelnour, T. (1978) . *In vivo* analysis of bone strain about the sagittal suture in *Macaca mulatta* during masticatory movements. *J. Dent. Res.* 57:904–908.

Bonfield, W., and Li, C.H. (1966). Deformation and fracture of bone. *J. Appl. Phys.* 37:869–875.

Brag, J. (1998). Chimpanzee variation facilitates the interpretation of the incisive suture closure in South African Plio-Pleistocene hominids. *Am. J. Phys. Anthopol.* 105:121–135.

Byron, C.D. (2006). Role of the osteoclast in cranial suture waveform patterning. *Anat. Rec.* 288A:552–563.

Byron, C.D., Borke, J., Yu, J., Pashley, D., Wingard, C.J., and Hamrick, M. (2004). Effects of increased muscle mass on mouse sagittal suture morphology and mechanics. *Anat. Rec.* 279A:676–684.

Byron, C.D., Hamrick, M.W., and Wingard, C.J. (2006a). Alterations of temporalis muscle contractile force and histological content from the myostatin and Mdx deficient mouse. *Arch. Oral Biol.* 51(5):396–405.

Byron, C.D., Hamrick, M., and Yu, J. (2006b). Cranial suture morphology: understanding how dietary strategy and brain size influence primate craniofacial bone growth (abstract). *Am. J Phys. Anthropol.* Suppl. 42:71.

Carmody, K.A., Mooney, M.P., Cooper, G.M., Bonar, C.J., Ciegel, M.I., and Smith, T.D. (2006). Bone cell dynamics of the premaxillary bone and its sutures (abstract). Am. *J. Phys. Anthropol.* Suppl. 42:73.

Carter, D.R., and Hayes, W.C. (1977). Compact bone fatigue damage—I. Residual strength and stiffness. *J. Biomech.* 10:325–337.

Chopra, S.R.K. (1957). The cranial suture closure in monkeys. *Pro. Zool. Soc.* London. 128:67–112.

Daegling, D.J. (1993). The relationship of *in vivo* bone strain to mandibular corpus morphology in *Macaca fascicularis*. *J. Hum. Evol.* 25:247–269.

Daegling, D., and Hotzman, J. (2003). Functional significance of cortical bone distribution in anthropoid mandibles: An *in vitro* assessment of bone strain under combined loads. *Am. J. Phys. Anthropol*. 122:38–50.

Daegling, D.J., and Hylander, W.L. (1998). Biomechanics of torsion in the human mandible. *Am. J. Phys. Anthropol.* 105:73–87.

Dechow, P.C., and Carlson, D.S. (1990). Occlusal force and craniofacial biomechanics during growth in rhesus monkeys. *Am. J. Phys. Anthropol*. 83:219–237.

Dechow, P.C., and Hylander, W.L. (2000). Elastic properties and masticatory bone stress in the macaque mandible. *Am. J. Phys. Anthropol*. 112:553–574.

Dechow, P.C., and Wang, Q. (2006). Strain gages. In:Webster, J.G.(ed.), *Encyclopedia of Medical Devices and Instrumentation*, 2nd edition, Vol. 6. Wiley, New Jersy, pp. 282–290.

Evans, F.G., and Lebow, M. (1951). Regional differences in some of the physical properties of the human femur. *J. Appl. Physiol*. 3:563–572.

Falk, D., Konigsberg, L., Helmkamp, R.C., Cheverud, J., Vannier, M., and Hildebolt, C. (1989). Endocranial suture closure in rhesus macaques (*Macaca mulatta*). *Am. J. Phys. Anthropol.* 80:417–428.

Gross, J. (1961). Aging of connective tissue, the extracellular components. In: Bourne, G.H., (ed.), *Structural Aspects of Aging*. Hafner Publishing Co. Inc., New York, pp:179–192.

Herring, S.W. (1972). Sutures – a tool in functional cranial analysis. *Acta Anatomica* 83: 222–247.

Herring, S.W. (1993). Epigenetic and functional influence on skull growth. In: Hanken, J. and Hall, B.K. (eds.), *The Vertebrate Skull*, Vol 1. University of Chicago Press, Chicago, pp 153–206.

Herring, S. W., and Mucci, R. J. (1991). *In vivo* strain in cranial sutures: the zygomatic arch. *J. Morphol*. 207:225–239.

Herring, S. W., and Rafferty, K. L. (2000). Cranial and facial sutures: functional loading in relation to growth and morphology. In: Davidovitch, Z. and Mah, J. (eds.), *Biological Mechanisms of Tooth Eruption, Resorption and Replacement by Implants*. Harvard Society for Advanced Orthodontics, Boston, pp 269–276.

Herring, S.W., and Teng, S. (2000). Strain in the braincase and its sutures during function. *Am. J. Phys. Anthropol*. 112:575–593.

Hershkovitz, I., Latimer, B., Dutour, O., Jellema, L.M., Wish-Baratz, S., Rothschild, C., and Rothschild, B.M. (1997). Why do we fail in aging the skull from the sagittal suture? *Am. J. Phys. Anthropol*. 103:393–399.

Hylander, W.L. (1979). Mandibular function in *Galago crassicaudatus* and *Macaca fascicularis*: an *in vivo* approach to stress analysis of the mandible. *J. Morphol.* 159:253–296.

Hylander, W.L. 1986. In vivo bone strain as an indicator of masticatory bite force in *Macaca fascicularis*. *Archs. Oral. Biol*. 31:149–157.

Hylander, W.L., and Johnson, K.R. (1997). *In vivo* bone strain patterns in the zygomatic arch of macaques and the significance of these patterns for functional interpretations of craniodental form. *Am. J. Phys. Anthropol*. 102:203–232.

Hylander, W.L., Johnson, K.R., and Crompton, A.W. (1992). Muscle force recruitment and biomechanical modeling: an analysis of masseter muscle function during mastication in *Macaca fascicularis*. *Am. J. Phys. Anthropol*. 88:365–387.

Hylander, W.L., Picq, P.G., and Johnson, K.R. (1991). Masticatory-stress hypotheses and the supraorbital region of primates. *Am. J. Phys. Anthropol.* 86:1–36.

Jaslow, C.R. (1990). Mechanical properties of cranial sutures. *J. Biomech*. 23:313–321.

Jaslow, C.R., and Biewener, A.A. (1995). Strain patterns in the horncores, cranial bones and sutures of goats (*Capra hircus*) during impact loading. *J. Zool*. 235:193–210.

Kokich, V.G. (1976). Age changes in the human frontozygomatic suture from 20 to 95 years. *Am. J. Orthod*. 69:411–430.

Krogman, W.M. (1930). Studies in growth changes in the skull and face of anthropoids: Ectocranial and endocranial suture closure in anthropoids and old world apes. *Am. J. Phys. Anthropol*. 46:315–353.

Lakes, R. (2001). Viscoelastic properties of cortical bone. In Cowin SC (ed.), Bone *Mechanical Handbook*, 2nd edition, Chapter 11. CRC, Bioca Raton, pp 1–15.

Leigh, S.R., and Shea, B.T. (1995). Ontogeny and the evolution of adult body size dimorphism in apes. *Am. J. Primatol*. 36:37–60.

Lieberman, D.E., Krovitz, G.E., Yates, F.W., Devlin, M., and Clairem M. St. (2004). Effects of food processing on masticatory strain and craniofacial growth in a retrognathic face. *J. Hum. Evol.* 46:655–677.

Liu, Z.J., and Herring, S.E. (2000). Bone surface strains and internal bony pressures at the jaw joint of the miniature pig during masticatory muscle contraction. *Archs. Oral. Biol.* 45:95–112.

Mao, J.J. (2002). Mechanobiology of craniofacial sutures. J. Dent. Res. 81:810–816.

Mao, J.J., Wang, X., and Kopher, R.A. (2003). Biomechanics of craniofacial sutures: orthopedic implications. *Angle Orthod*. 732:128–135**.**

Marinescu, R., Daegling, D.J., and Rapoff, A.J. (2005). Finite-element modeling of the anthropoid mandible: The effects of altered boundary conditions. *Anat. Rec*. 283A:300–309.

Massler, M., and Schour, I. (1951). The growth pattern of the cranial vault in the albino rat as measured by vital staining with alizarine red "S". *Anat. Rec*. 110:83–101.

Milch, R.A. (1966). Aging of connective tissues. In: Schock, N.W. (ed.), *Perspectives in Experimental Gerontology*. Charles C Thomas, Springfield, pp 109–124.

Miroue, M., and Rosenberg, L. (1975). *The Human Facial Sutures: A Morphological and Histological Study of Age Changes from 20 to 95 Years*. M.S.D. thesis, University of Washington.

Mooney, M.P., and Siegel, M.I. (1991). Premaxillary-maxillary suture fusion and anterior nasal tubercle morphology in the chimpanzee. *Am. J. Phys. Anthropol*. 85:451–456.

Oudhof, H.A., and van Doorenmaalen, W.J. (1983). Skull morphogenesis and growth: hemodynamic influence. *Acta. Anat*. (Basel) 117:181–186.

Radhakrishnan, P., and Mao, J.J. (2004). Nanomechanical properties of facial sutures and sutural mineralization front. *J. Dent. Res*. 83:470–475.

Rafferty, K.L., and Herring, S.W. (1999). Craniofacial sutures: morphology, growth, and *in vivo* masticatory strains. *J. Morph*. 242:167–179.

Rafferty, K.L., Herring, S.W., and Marshall, C. (2003). The biomechanics of the rostrum and the role of facial sutures. *J. Morph*. 257:33–44.

Ravosa, M.J., Johnson, K.R., and Hylander, W.L. (2000). Strain in the galago facial skull. *J. Morphol*. 245:51–66.

Richmond, B.G., Wright, B., Grosse, I., Dechow, P.C., Ross, C.F., Spencer, M.A., and Strait, D.S. (2005). Finite element analysis in functional morphology. *Anat. Rec*. 283A:259–274.

Ross, C.F. (2001). *In vivo* function of the craniofacial haft: the interorbital pillar. *Am. J. Phys. Anthropol.* 116:108–139.

Ross, C.F., and Hylander, W.L. (1996.) *In vivo* and *in vitro* bone strain in the owl monkey circumorbital region and the function of the postorbital septum. *Am. J. Phys. Anthropol.* 101:183–215.

Ross, C.F., and Metzger, K.A. (2004). Bone strain gradients and optimization in vertebrate skulls. *Ann. Anat*. 186:387–396.

Ross, C.F., Strait, D.S., Richmond, B.G., and Spencer, M.A. (2002). *In vivo* bone strain and finite-element modeling of the anterior root of the zygoma in *Macaca* (abstract). *Am. J. Phys. Anthropol.* Suppl. 34:133.

Smith, K.K., and Hylander, W.L. (1985). Strain Gage measurement of mesokinetic movement in the lizard *Varanus exanthematicus*. *J. Exp. Biol*. 114:53–70.

Strait, D.S., Wang, Q., Dechow, P.C., Ross, C.F., Richmond, B.G., Spencer, M.A., and Patel, B.A. (2005). Modeling elastic properties in finite element analysis: How much precision is needed to produce an accurate model? *Anat. Rec*. 283A:275–287.

Thayers, T.A. (1990). Effects of functional versus bisected occlusal planes on the "Wits" appraisal. *Am. J. Orthod. Dentofacial Orthop*. 97:422–426.

Wang, Q., and Dechow, P.C. (2006). Elastic properties of external cortical bones in the craniofacial skeletons of the rhesus monkey. *Am. J. Phys. Anthropol*. 131:402–415.

Wang, Q., Opperman, L.A., Havill, L.M., Carlson, D.S., and Dechow, P.C. (2006a). Inheritance of sutural patterns at pterion in rhesus monkeys skulls. *Anat. Rec*. 288A:1042–1049.

Wang, Q., Strait, D.S., and Dechow, P.C. (2006b). Fusion patterns of craniofacial sutures in rhesus monkey skulls of known age and sex from Cayo Santiago. *Am. J. Phys. Anthropol*. 131:469–485.

Wang, Q., Strait, D.S., and Dechow, P.C. (2006c). A comparison of cortical elastic properties in the craniofacial skeletons of three primate species and its relevance to human evolution. *J. Hum. Evol*. 51:375–382.

Wright, B., Richmond, B.G., Strait, D.S., Ross C.F., Spencer, M.A., Wang Q., and Dechow P.C., (n.d.). Finite element analysis of bite point location and craniofacial strain using a macaque model. *Am. J. Phys. Anthropol*. (In review).

Yamashita, J., Wang, Q., and Dechow, P.C. (2006). Biomechanical effects of fixed partial denture therapy on strain patterns of the mandible. *J. Prosthet. Dent*. 95:55–62.

Zar, J.H. (1999). *Biostatistical Analysis*. 4th edition. Prentice Hall, Upper Saddle River, New Jersey.